RESEARCH ARTICLE

NANO · MICRO small
www.small-journal.com

Mulberry Leaf Lipid Nanoparticles: a Naturally Targeted CRISPR/Cas9 Oral Delivery Platform for Alleviation of Colon Diseases

Lingli Ma, Ya Ma, Qiang Gao, Shengsheng Liu, Zhenhua Zhu, Xiaoxiao Shi, Fangyin Dai, Rui L. Reis, Subhas C. Kundu, Kaiyong Cai,* and Bo Xiao**

Oral treatment of colon diseases with the CRISPR/Cas9 system has been hampered by the lack of a safe and efficient delivery platform. Overexpressed CD98 plays a crucial role in the progression of ulcerative colitis (UC) and colitis-associated colorectal cancer (CAC). In this study, lipid nanoparticles (LNPs) derived from mulberry leaves are functionalized with Pluronic copolymers and optimized to deliver the CRISPR/Cas gene editing machinery for CD98 knockdown. The obtained LNPs possessed a hydrodynamic diameter of 267.2 nm, a narrow size distribution, and a negative surface charge (−25.6 mV). Incorporating Pluronic F127 into LNPs improved their stability in the gastrointestinal tract and facilitated their penetration through the colonic mucus barrier. The galactose end groups promoted endocytosis of the LNPs by macrophages via asialoglycoprotein receptor-mediated endocytosis, with a transfection efficiency of 2.2-fold higher than Lipofectamine 6000. The LNPs significantly decreased CD98 expression, down-regulated pro-inflammatory cytokines (TNF-α and IL-6), up-regulated anti-inflammatory factors (IL-10), and polarized macrophages to M2 phenotype. Oral administration of LNPs mitigated UC and CAC by alleviating inflammation, restoring the colonic barrier, and modulating intestinal microbiota. As the first oral CRISPR/Cas9 delivery LNP, this system offers a precise and efficient platform for the oral treatment of colon diseases.

1. Introduction

Ulcerative colitis (UC) is a chronic, recurrent inflammatory disorder of the colon, whose clinical manifestations include mucosal inflammation, diarrhea, and blood in the stool. Long-term inflammation drives the occurrence and progression of colitis-associated cancer (CAC), and no effective clinical treatment is available for these colon diseases.[1] Recently, the clustered regularly interspaced short palindromic repeats (CRISPR)/CRISPR-associated protein 9 (Cas9) system has been exploited as a powerful gene-editing technique for precisely regulating genes,[2] with great potential for the treatment of various diseases, such as atherosclerosis,[3] infection, and cancer.[4] However, delivery of the CRISPR/Cas gene-editing machinery is the critical rate-limiting step in its applications because of limited payload, poor delivery efficiency, and potential adverse effects.[5]

The gene-editing complex must be loaded into carriers that protect it from

L. Ma, Y. Ma, Q. Gao, S. Liu, X. Shi, F. Dai, B. Xiao
State Key Laboratory of Resource Insects
College of Sericulture, Textile, and Biomass Sciences
Southwest University
Chongqing 400715, China
E-mail: fydai@swu.edu.cn; bxiao@swu.edu.cn

Z. Zhu
Department of Gastroenterology
The First Affiliated Hospital of Nanchang University
Nanchang 330006, China

R. L. Reis, S. C. Kundu
Bs Research Group
I3Bs — Research Institute on Biomaterials
Biodegradables and Biomimetics
Headquarters of the European Institute of Excellence on Tissue
Engineering and Regenerative Medicine
University of Minho
AvePark, Barco, Guimaraes 4805-017, Portugal

The ORCID identification number(s) for the author(s) of this article can be found under https://doi.org/10.1002/smll.202307247

DOI: 10.1002/smll.202307247

R. L. Reis, S. C. Kundu
ICVS/3B's-PT Government Associate Laboratory
Braga, Guimarães 4800-058, Portugal

K. Cai
Key Laboratory of Biorheological Science and Technology
Ministry of Education
College of Bioengineering
Chongqing University
Chongqing 400044, China
E-mail: kaiyong_cai@cqu.edu.cn

the harsh biological environment, assist in transferring it across the plasma membrane of target cells, and allow it to escape from the lysosomes into the cytoplasm. Non-viral vectors, including dendritic polymers, polymeric nanoparticles (NPs), and mesoporous silica NPs, have recently been tested to deliver CRISPR/Cas tools.[6] Among these nonviral vectors, lipid NPs (LNPs) are the first to be used for delivering the gene editing system,[7] which are the only clinically approved carrier for the delivery of nucleic acids due to their high loading capacity for hydrophilic macromolecules, ease of scalable production, and biosafety.[8] Siegwart et al. constructed modified LNPs to deliver Cas9/sgRNA ribonucleoprotein complexes into target tissues. After intravenous injection, these LNPs accumulated in the lungs and efficiently edited six genes therein.[9] Subsequently, Qiu et al. produced a novel artificial LNP and encapsulated Cas9 messenger RNA and guide RNA for in vivo genome editing of *Angptl3*. Mouse experiments revealed that these LNPs enabled specific knockdown of the *Angptl3* gene in the liver, reducing serum ANGPTL3, cholesterol, and triglyceride levels.[10] Han and colleagues recently prepared optimized LNPs to deliver Cas9 mRNA and sgRNA targeting antithrombin.[11] These LNPs inhibited antithrombin production in the liver and improved thrombin generation, alleviating hemophilia A and B. Despite the promising results of these LNPs in delivering CRISPR/Cas gene-editing machinery, all these studies were based on the intravenous injection of LNPs.

The oral route has been considered the best approach for drug administration because of increased patient compliance, convenient self-administration, and direct drug delivery to the diseased colon tissues.[12] Unfortunately, the acidic gastric conditions, the digestive enzymes, and abundant microbes in the gastrointestinal tract (GIT) exerted a negligible effect on the stability of NPs.[13] Recently, we extracted exosome-like LNPs from edible plants (e.g., tea flower, tea leaf, and ginger) and found that they could maintain stability in the GIT and accumulate in the colonic lesion tissues.[14] Thus, these natural LNPs entered human clinical trials to prevent and treat various diseases, such as oral mucositis, polycystic ovary syndrome, and colon cancer (https://clinicaltrials.gov). In the present study, we describe a novel LNP for oral delivery of genome editing machinery to down-regulate the expression of CD98 in the inflamed colon. The LNPs (P_{127}M@pCD98s) were derived from mulberry leaf lipids (MLLs) with the addition of an FDA-approved polymer (Pluronic F127, P_{127}) (**Scheme 1a**). After oral administration, they traveled through the upper GIT, infiltrated through the colonic mucus barrier, and penetrated the colitis tissues with the assistance of P_{127}. Thereafter, they were internalized by colonic epithelial cells and macrophages mediated by galactose end groups of MLLs. The CRISPR/Cas plasmid against *CD98* (pCD98) was released from P_{127}M, activated its *CD98* editing function, and achieved desired therapeutic outcomes against UC and CAC (Scheme 1b).

2. Results and Discussion

2.1. Fabrication and Physicochemical Characterizations of LNPs

Edible plants contain large amounts of macromolecules like polysaccharides, lipids, and proteins that can be used as drug carriers. In the present study, glycolipids were extracted and purified from mulberry leaves. The MLLs were mainly composed of triglyceride (TG, 24.9%), phosphatidylethanolamine (PE, 17.0%), and monoacylglycerol (MG, 9.9%), as shown in Table S1 and **Figure 1a** (Supporting Information). We found that MLLs contained several types of galactose-bearing glycolipids, including monogalactosyl-monoacylglycerol (MGMG), digalactosyl-monoacylglycerol (DGMG), and monogalactosyl-diacylglycerol (MGDG). As reported, macrophages are one of the most crucial target cells for treating UC and CRC, and their surfaces are abundantly decorated with galactose-type lectins;[15] therefore, MLL-based LNPs were expected to possess the capacity for specific drug delivery to macrophages.

LNPs were produced from MLLs by a thin-film hydration method. Their hydrodynamic particle size varied from 187.2 to 529.7 nm during incubation in simulated colonic fluid (SCF) (Figure 1b), suggesting they were unstable in the colon lumen. To address this issue, FDA-approved amphiphilic Pluronic polymers were used to reinforce the LNPs. In principle, the hydrophobic poly(propylene oxide) sections of the Pluronic polymers were integrated into the hydrophobic lipid bilayer of the LNPs driven by the "like dissolves like" rule. At the same time, their hydrophilic polyethylene glycol (PEG) segments extended to the LNP surface. We compared the stabilizing effectiveness of various Pluronic polymers (L_{65}, P_{68}, P_{108}, P_{123}, and P_{127}; Figure 1c) on MLL-based LNPs, and the weight ratio of Pluronic polymer to MLL was set at 5:100 (w/w). It was observed that P_{127}-modified MLL-based LNPs (P_{127}Ms) showed minimal size variation (174.3 – 270.0 nm) in the SCB, and P_{127} was thus selected as the stabilizing agent in subsequent experiments. LNPs contain aqueous cavities capable of loading hydrophilic compounds (e.g., plasmids, siRNAs, and miRNAs). To determine the appropriate MLL/pCD98 weight ratio, an agarose gel retardation assay was carried out. Figure 1d revealed that free pCD98 molecules with negative charges moved to the positive pole in the electric field. When the weight ratios were below 30, pCD98 was partially released from P_{127}M@pCD98s and migrated into the agarose gel. Meanwhile, we found that weight ratios $\geq$ 30 resulted in no premature release of pCD98, indicating that the encapsulation efficiency of pCD98 in P_{127}Ms was close to 100% at the weight ratios of pCD98/MLL over 30. Therefore, the MLL/pCD98 weight ratio was set at 30 for subsequent investigations.

NPs will encounter the harsh environment of the GIT after oral administration, and they must maintain stability under those conditions. Accordingly, we determined the stability of MLL-based LNPs, P_{127}Ms, and P_{127}M@pCD98s in buffers simulating different sections of the GIT. MLL-based LNPs were unstable during incubation in the simulated gastric fluid (SGF), simulated intestinal fluid (SIF), and SCF, as demonstrated by changes in particle sizes, polydispersity index (PDI) values, and zeta potentials (Figure 1e). On the contrary, the particle sizes and size distributions of P_{127}Ms and P_{127}M@pCD98s remained stable in the simulated gastrointestinal fluids, demonstrating the necessary stability for oral administration. In addition, the morphology of P_{127}M@pCD98s was determined by transmission electron microscopy (TEM). It was observed that these LNPs appeared spherical with an average diameter of 227.8 nm (Figure 1f), which had conspicuous lipid-bilayer membranes (Figure S1, Supporting Information). We also found that P_{127}M@pCD98s had an

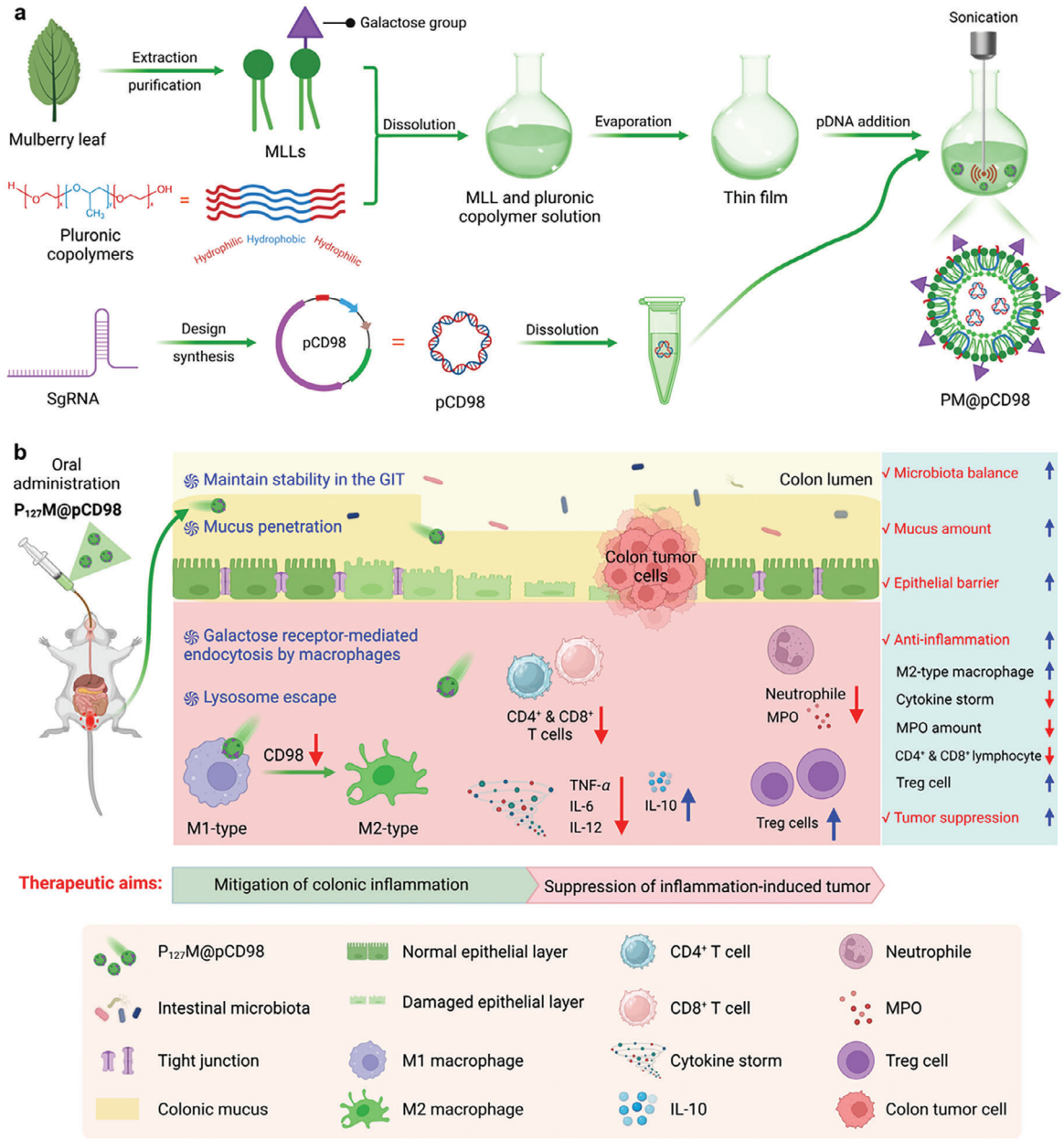

Scheme 1. Fabrication and therapeutic mechanisms of P127M@pCD98s against colon diseases. a) Schematic diagram of the fabrication procedure of PM@pCD98s. b) Schematic illustration of oral P127M@pCD98s to target deliver CRISPR/Cas gene editing machinery for CD98 knockdown and exert therapeutic effects against UC and CAC. After oral administration, P127M@pCD98s maintain stability in the stomach and small intestine, penetrate through the mucus layer, accumulate in the inflamed colon tissues, are internalized by colon epithelial cells and macrophages via galactose receptor-mediated endocytosis, and release the loaded pCD98 to the cytoplasm. After that, these LNPs knockdown CD98 expression, decrease inflammatory responses, increase mucus amount, protect the colonic epithelial barrier, suppress colon tumor growth, and modulate intestinal microbiota, eventually resulting in effective treatment of UC and CAC. This figure was created with BioRender.com.

average hydrodynamic particle size of 267.2 nm, a narrow size distribution (PDI = 0.205), and negative surface charge (−25.6 mV) (Figure 1g,h). The average particle size of P_{127}M@pCD98s determined by TEM was considerably less than that measured by dynamic light scattering (DLS), which might be attributed to the shrinkage of LNPs as a result of drying for TEM compared with the swollen state of LNPs during DLS examination.

2.2. In Vitro Cell Internalization by Macrophages, Lysosomal Escape, and Gene Transfection Efficiency of LNPs

In vitro biosafety of nanotherapeutics is a critical prerequisite for their biomedical applications, and this property of P_{127}M@pCD98s was determined against macrophages. After incubation with LNPs (pCD98, 1 μg mL^{-1}) for 24 h, peritoneal macrophages were examined for apoptosis by staining with

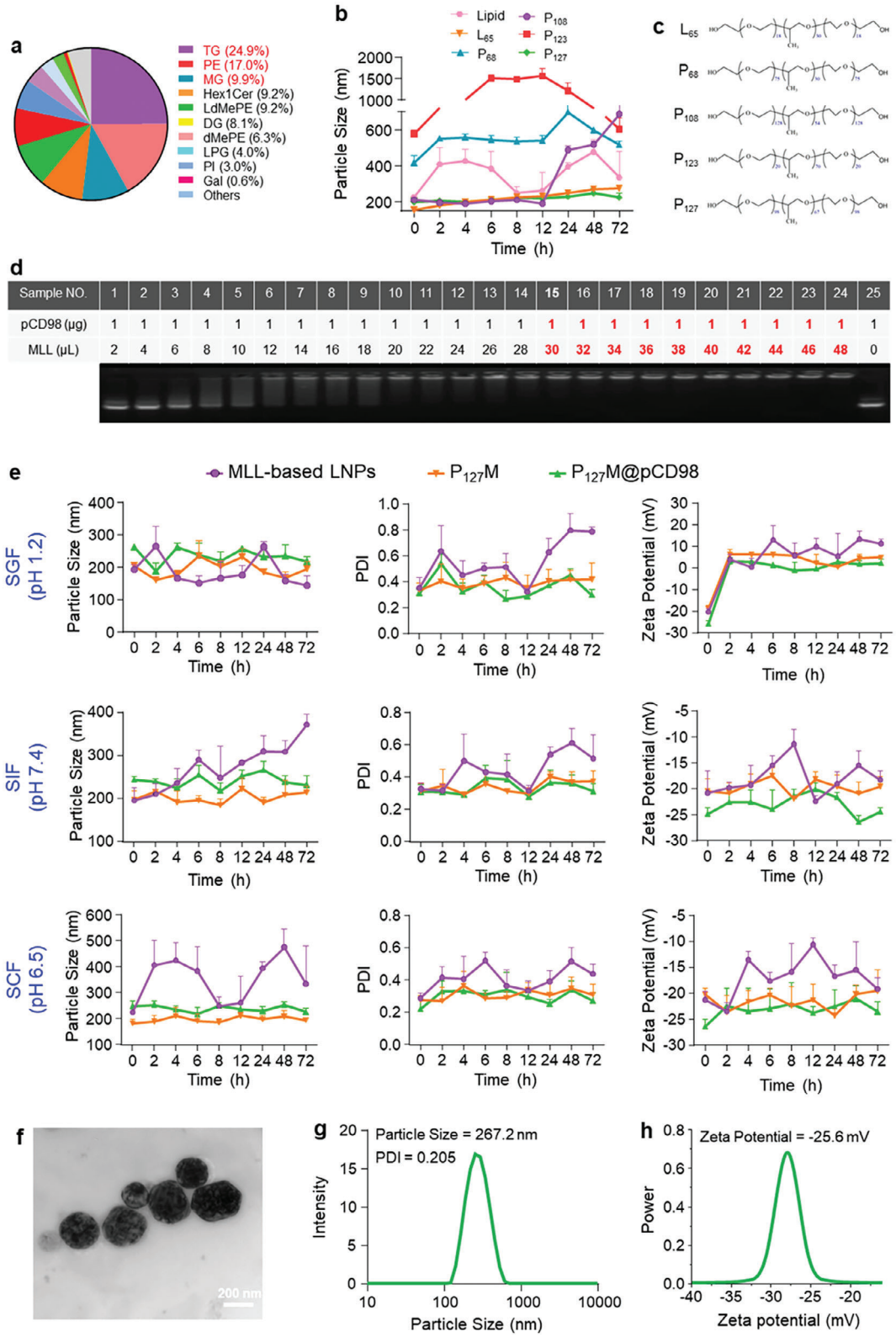

Figure 1. Physicochemical characterizations of various LNPs. a) Lipid compositions of MLLs. b) Particle size variations of LNPs containing different Pluronic copolymers in SCB. Each point represents mean ± S.E.M. (n = 3). c) Molecular structures of various Pluronic copolymers. d) Agarose gel electrophoresis of P_{127}M@pCD98s with different MLL/pCD98 weight ratios. e) Stability of LNPs in various buffers simulating the pH environment of the stomach (pH 1.2), small intestine (pH 7.4), and colon (pH 6.5), respectively. Each point represents mean ± S.E.M. (n = 3). f) A representative TEM image of P_{127}M@pCD98s (scale bar = 200 nm). g) Hydrodynamic particle size distribution and h) zeta potential of P_{127}M@pCD98s.

annexin V-FITC/propidium iodide (Vybrant, Thermo Fisher). As shown in Figure S2 (Supporting Information), a small percentage of necrotic and apoptotic cells were observed in the control group (1.9%) and the P_{127}M@pCD98-treated group (9.0%), while macrophages treated with Lipofectamine 6000 (Lipo6000)/pCD98 complexes had a larger proportion of apoptotic cells (48.4%). These results confirm that P_{127}Ms show much better biocompatibility than Lipo6000, a new commercial gene transfection reagent with high efficiency.

Because plasmids exert their therapeutic functions within cells, they are required to be internalized in the target cells.[16] Initially, P_{127}Ms were labeled with the lipophilic green fluorescent dye, DiO, to track their intracellular distribution; the cell internalization profiles were qualitatively and quantitatively evaluated by laser confocal scanning microscopy (CLSM) and flow cytometry (FCM), respectively. As displayed in **Figure 2a**, the control cells showed negligible green fluorescence, while obvious DiO signals were detected in the P_{127}M@DiO-treated cells. FCM results revealed that the uptake percentages of LNPs by macrophages were 29.2%, 78.8%, and 99.3% after co-incubation for 1, 3, and 5 h, respectively (Figure 2b), implying a time-dependent cellular uptake profile of LNPs. As reported, C-type galactose receptors (galactose-type lectins) were found to be overexpressed on the surface of activated macrophages in the inflammatory microenvironment.[17] It is worth noting that several types of glycolipids in P_{127}Ms are end-capped with natural galactose moieties, which might endue LNPs with intrinsic macrophage-targeting potential.[16] To test this hypothesis, we comparatively quantified the cellular uptake efficiencies of P_{127}M@DiOs in the media with or without free galactose, which acted as a molecular competitor for end-capped galactose on the LNP surface. Free galactose significantly decreased the cell internalization efficiency of P_{127}M@DiOs to 13.7%, 33.0%, and 61.8% after incubation for 1, 3, and 5 h, respectively, suggesting that P_{127}Ms were internalized by activated macrophages via galactose receptor-mediated endocytosis.

Over 90% of internalized nucleic acids are degraded in the lysosomes. Thus, lysosome escape has been considered a crucial bottleneck for their delivery. To benchmark the lysosome escape capacity of P_{127}Ms, the endolysosomal compartments were stained with LysoTracker Red. After incubation for 1 or 4 h, LNPs were efficiently internalized by Raw 264.7 macrophages, and the green LNP signals mostly overlapped with the red endolysosomal organelle signals, indicated by yellow spots (Figure 2c). With increasing incubation time (8 h), more green signals appeared in the interiors of cells, revealing successful escape of LNPs from the lysosomes. We found that the Pearson correlation coefficients (PCCs) of the P_{127}M@FITC-siRNA-treated cells were 0.542, 0.398, and 0.204 after incubation for 1, 4, and 8 h, respectively. The preceding findings demonstrate that P_{127}Ms can be efficiently internalized by macrophages and undergo lysosomal escape within 8 h. Given their high efficiencies of cellular uptake and lysosomal escape, P_{127}Ms were expected to facilitate the expression of exogenous genes. To test this expectation, we loaded pGFP into P_{127}Ms and determined its expression levels (Figure 2d,e). It was found that 71.2% of the P_{127}M@pGFP (pGFP, 1 μg mL^{-1})-treated macrophages presented green fluorescence after co-incubation for 48 h, which was 2.2-fold higher than cells incubated with Lipo6000@pGFPs (pGFP, 1 μg mL^{-1}).

2.3. In Vitro CD98 Gene Editing in Macrophages and Anti-Inflammatory Activity of LNPs

Since P_{127}Ms were efficiently internalized by macrophages and escaped from lysosomes, we further investigated *CD98* editing efficiency of P_{127}M@pCD98s in Raw 264.7 macrophages using quantitative reverse-transcription polymerase chain reaction (qRT-PCR), and the primers were shown in Table S2 (Supporting Information). P_{127}Ms (without pCD98) slightly decreased CD98 mRNA expression to 80.9% compared with control cells, while the CD98 mRNA level in the P_{127}M@pCD98-treated group was reduced to 38.8% (Figure S3, Supporting Information). This result might be attributed to the synergistic effect of P_{127}Ms and pCD98 in down-regulating CD98 expression. It was found that LPS treatment significantly increased CD98 mRNA expression (Figure 2f), and P_{127}M@pCD98 treatment down-regulated CD98 mRNA expression to the average level of the negative control.

Macrophages play a crucial role in the development of inflammatory and autoimmune diseases.[18] Therefore, we determined whether *CD98* editing could mitigate the inflammatory responses of activated macrophages. It can be seen in Figure 2g that the positive control (0.5 μg mL^{-1} LPS) showed a much higher TNF-α concentration (458.3 pg mL^{-1}) than the negative control (137.2 pg mL^{-1}). However, the P_{127}M@pCD98 treatment (160.4 pg mL^{-1}) induced a TNF-α concentration comparable to the negative control. The changes in IL-6 concentrations presented the same trend as those of TNF-α (Figure 2h), and treatment with P_{127}M@pCD98s significantly increased IL-10 levels (Figure 2i). These observations demonstrate that *CD98* editing is a viable strategy for down-regulating the pro-inflammatory cytokines (TNF-α and IL-6) and up-regulating the anti-inflammatory cytokine (IL-10), which may retard the development of colonic inflammation and CRC.

Macrophages can be converted to the pro-inflammatory M1-type or the anti-inflammatory M2-type by the stimulations of environmental factors,[19] such as cell debris, bacterial products, and lymphocytes.[20] It has been demonstrated that macrophage transformation from M1-type to M2-type improved UC treatment efficacies.[21] As shown in Figure 2j,k and Figure S4 (Supporting Information), LPS treatment increased the level of the M1 macrophage marker (iNOS), while incubation with P_{127}M@pCD98s or IL-10 reduced iNOS compared with the positive LPS control. Variations in the M2 macrophage marker (CD206) presented an opposite trend to those of iNOS (Figure 2j,l; Figure S4, Supporting Information), confirming that P_{127}M@pCD98s facilitated macrophage polarization to the M2 phenotype.

2.4. In Vitro Cellular Uptake, Lysosomal Escape, and *CD98* Editing of LNPs in Colonic Epithelial Cells

The uptake (Figure S5, Supporting Information), lysosomal escape (Figure S6, Supporting Information), and gene transfection efficiency (Figure S7, Supporting Information) of P_{127}Ms in CT-26 cells were similar to those in macrophages, so we evaluated whether P_{127}M@pCD98s could edit CD98 expression in CT-26 cells, a typical colorectal carcinoma cell line. Figure S8a (Supporting Information) revealed that P_{127}Ms (without

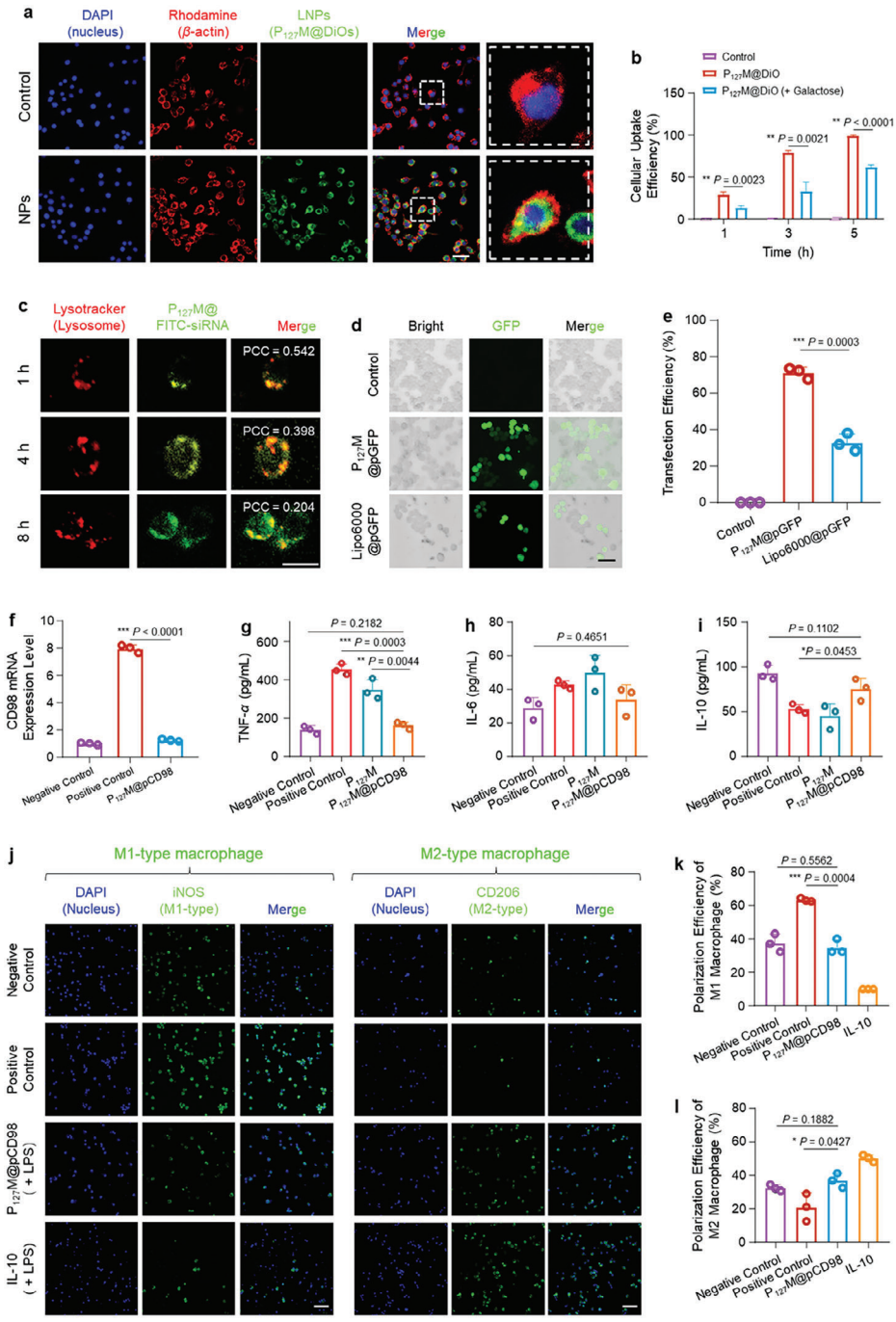

Figure 2. In vitro cell internalization and anti-inflammatory activities of various LNPs. a) CLSM images of Raw 264.7 macrophages with the treatment of P127M@DiOs for 5 h (scale bar = 50 μm). Macrophages were stained with DAPI and Rhodamine-labeled phalloidin to visualize the nuclei (blue) and cytoskeletons (red), respectively. b) Macrophage internalization efficiencies of P127M@DiOs in the presence and absence of galactose at different time points (1, 3, and 5 h). c) CLSM images of Raw 264.7 macrophages with the treatment of P127M@DiOs (DiO, 10 μM) for 1, 4, and 8 h, respectively (scale bar = 20 μm). Macrophages were stained with LysoTracker Red for visualization of lysosomes (red). d) CLSM images of Raw 264.7 macrophages with the treatment of P127M@pGFPs and Lipo6000@pGFPs at an equal pGFP concentration of 1 μg/mL for 48 h (scale bar = 50 μm). e) Quantification of transfection efficiencies of P127M@pGFPs (pGFP, 1 μg mL^{-1}) and Lipo6000@pGFPs (pGFP, 1 μg mL^{-1}) in Raw 264.7 macrophages after co-incubation for 48 h. f) CD98 mRNA expression levels of Raw 264.7 macrophages exposed to LNPs (pCD98, 1 μg mL^{-1}) for 48 h. Macrophages without treatments were used as a negative control, whereas LPS-treated macrophages were used as a positive control. The concentrations of (g) TNF-α, h) IL-6, and (i) IL-10 in the supernatants of Raw 264.7 macrophages after treatment of different LNPs (pCD98, 1 μg mL^{-1}). (j) CLSM images of iNOS (a biomarker for M1-phenotype macrophage) and CD206 (a biomarker for M2-phenotype macrophage) in Raw 264.7 macrophages after different treatments for 24 h (Scale bar = 100 μm). Percentages of (k) M1-phenotype and (l) M2-phenotype macrophages after different treatments for 24 h using Image J software. Each point represents mean ± S.E.M. (n = 3; $^{*}p < 0.05$, $^{**}p < 0.01$, $^{***}p < 0.001$, and ns = no significance).

pCD98) slightly decreased the CD98 mRNA level relative to the control cells. This observation can be attributed to the anti-inflammatory lipids (e.g., phosphatidylserine and phosphatidylcholine) in P_{127}Ms, and these lipids can down-regulate the inflammatory level and inflammation-associated CD98. We further found that P_{127}M@pCD98s produced a noticeable reduction in CD98 mRNA compared to controls (61.3% decrease after incubation for 48 h). The overexpression of programmed cell death ligand 1 (PD-L1) helps malignant cells evade attack by $CD8^+$ T cells from the host immune system through the interaction with PD-1 receptors.[22] Accordingly, we determined the PD-L1 expression level in CT-26 cells after *CD98* editing (Figure S8b, Supporting Information). The reduction in CD98 expression significantly decreased the PD-L1 mRNA level to 26.3% of the control level, suggesting that CD98 could regulate the expression of PD-L1, whose knockout might be beneficial for mitigating CRC.

2.5. Mucus Penetration and In Vivo Biodistribution of LNPs

Goblet cells at the luminal side of the colon continuously produce and secrete the highly glycosylated mucin, MUC2.[23] This glycoprotein acts as a core molecule to construct protective viscoelastic mucus, which separates the colonic epithelial layer from extraneous matters (e.g., intestinal bacteria, food particles, and metabolic waste products),[24] entraps these substances, and facilitates their distal transport by intestinal peristalsis and mucus turnover.[25] Evidence indicates that mucus is an important obstacle for oral drug delivery to the diseased colon tissue.[26] Therefore, we determined the mucus-penetrating property of P_{127}Ms using a hydroxyethyl cellulose (HEC) hydrogel to simulate the mucosal barrier. The HEC hydrogel was labeled with rhodamine, and P_{127}Ms were loaded with DiO to track their distributions. Compared with M@DiOs (without P_{127}), P_{127}M@DiOs showed much deeper mucus penetration (**Figure 3a,b**). Quantitative results revealed that after incubation in the simulated mucus for 10 min, the penetration depth of P_{127}M@DiOs was 3.3-fold higher than that of NPs without P_{127}, confirming that the introduction of P_{127} to LNPs endowed them with high mucus penetration capacity (Figure 3c).

To track the in vivo biodistribution of P_{127}Ms, DiR, a near-infrared (NIR) probe, was loaded into these LNPs. As seen in Figure 3d, weak NIR fluorescence was detected in the GIT from the control group due to tissue autofluorescence. The colon tissues from mice receiving oral administration of P_{127}M@DiRs presented the most vigorous NIR fluorescence intensity at 24 h, and the NIR intensity gradually weakened with the passage of time (Figure 3e). The five principal organs showed similar variation trends in NIR fluorescence intensities. 72 h after oral administration, the NIR intensities of all tested organs (GIT and five principal organs) decreased to the control base line, demonstrating that P_{127}M@DiRs could be eliminated from the GITs. We also determined the accumulation profiles of LNPs in the colitis tissues. At 24 h, the colon tissues were collected, embedded in optimal cutting temperature (OCT) compound, sectioned, and examined with a fluorescence microscope. It was observed that P_{127}M@DiOs (green) gradually accumulated in the colitis tissue (Figure 3f). To confirm the in vivo gene transfection efficiency of P_{127}Ms, the expression profiles of GFP in the colitis tissues were evaluated. As seen in Figure S9a,b, GFP was obviously expressed in the inflamed colon tissues after oral administration of P_{127}M@pGFPs for 24 and 48 h.

To determine whether P_{127}Ms maintained their macrophage-targeting ability in vivo, tissue sections were simultaneously stained with 4', 6-diamidino-2-phenylindole (DAPI) and Alexa Fluor 647 (AF647)-labeled F4/80 antibodies. It can be seen in Figure 3g that many green fluorescence signals (P_{127}M@DiOs) were co-localized with red fluorescence signals (F4/80 antibody-stained macrophages) in both colitis and CAC tissue sections. The in vivo macrophage-targeting capacity of P_{127}Ms was further confirmed by the obvious overlaps of the green fluorescence signals of GFP and the red fluorescence signals of macrophages (Figure S9c, Supporting Information). These results demonstrate that oral P_{127}Ms can efficiently traverse the colonic mucus layers, pass through the damaged colonic epithelial layer, accumulate in the UC/CAC tissues, and be specifically internalized by macrophages, supporting the necessary premise for the therapeutic effectiveness of the CRISPR/Cas gene-editing machinery.

2.6. In Vivo Retardation Effect of LNPs on Acute UC

Given the desirable physicochemical property, anti-inflammatory capacity, and accumulative potential in the UC/CAC mucosa of oral P_{127}M@pCD98s, we investigated their ability to ameliorate the harmful effects of dextran sulfate sodium (DSS)-induced acute UC (**Figure 4a**). Healthy control mice exhibited increased body weight (18.9%), while the DSS control showed a sharp decrease (17.5%) (Figure 4b). Oral administration of P_{127}Ms, P_{127}M@pCD98s (L, 1 μg pCD98/mouse), and P_{127}M@pCD98s (H, 5 μg pCD98/mouse) efficiently mitigated body weight losses. Strikingly, the body weight of the P_{127}M@pCD98 (H) group increased over 7.0% by the end of the investigation (day 21). The severity of acute colitis was assessed by the typical parameters of colon lengths, myeloperoxidase (MPO) activities, spleen indices, and inflammatory cytokine levels. The healthy control mice and the DSS control mice showed the longest (5.5 cm) and the shortest (3.4 cm) colon lengths, respectively. The colon lengths in the P_{127}M@pCD98 (H) group were comparable to those in the healthy control (Figure 4c; Figure S10, Supporting Information). MPO, mainly secreted by active neutrophils, is a critical indicator of inflammation in the colitis tissues;[27] spleen weight is increased due to the activation, proliferation, and accumulation of immune cells during UC progression.[28] P_{127}M@pCD98 (H) treatment retarded the increasing trend of MPO activities (Figure 4d) and spleen weights (Figure 4e), but no statistically significant difference was detected in these two parameters between the healthy control and the P_{127}M@pCD98 (H) group. The groups receiving oral treatment of various LNPs did show decreased levels of pro-inflammatory cytokines (TNF-α and IL-6) compared with the DSS control (Figure 4f,g), while an opposite trend was seen for IL-10 (Figure 4h).

To investigate the inflammatory status and histological damage of colon tissues, they were sectioned and stained with

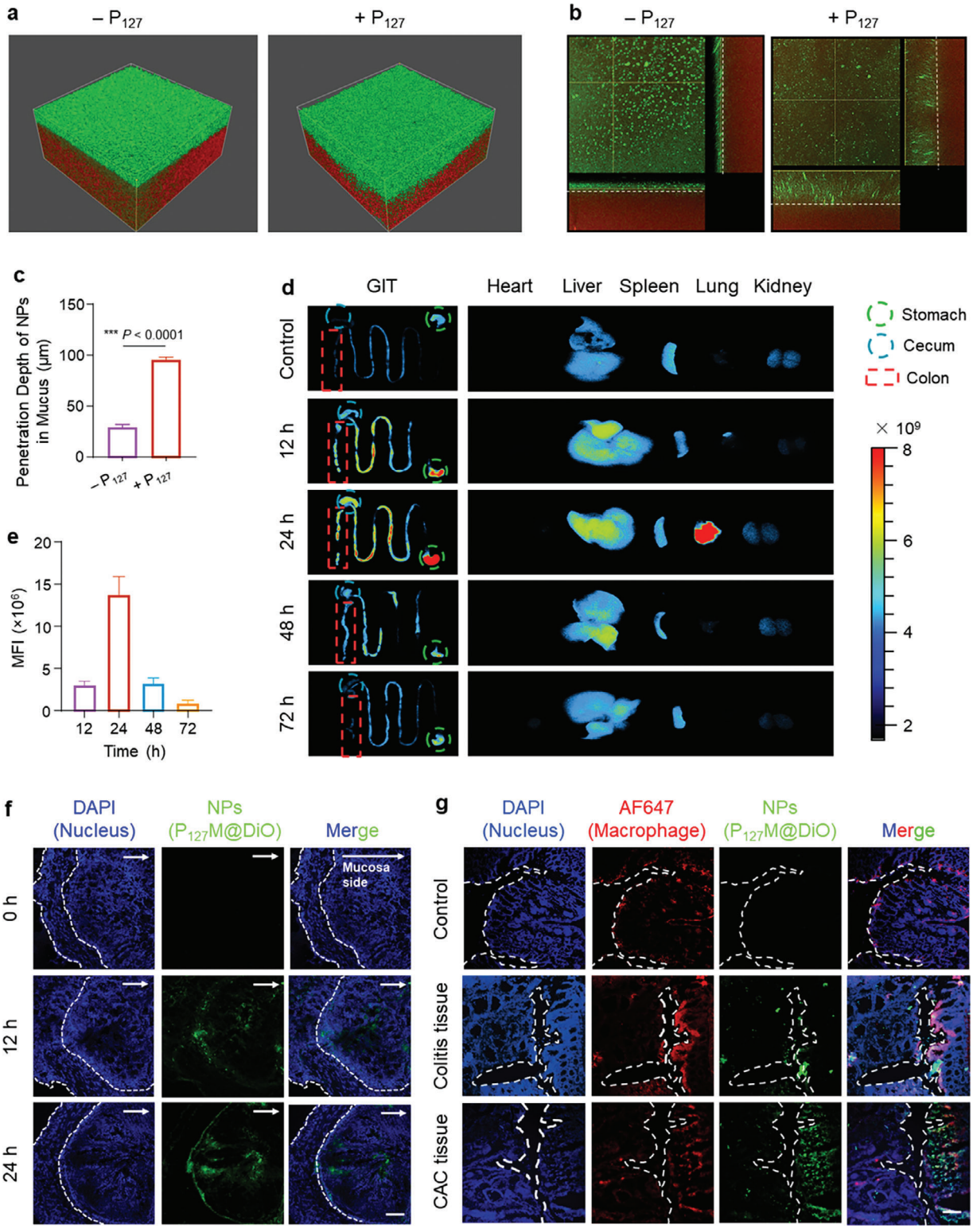

Figure 3. Mucus penetration and in vivo bio-distribution profiles of various LNPs. a) 3D fluorescence images, b) sectional fluorescence images, and c) the corresponding quantitative penetration depths of MLL-based LNPs with or without P127. d) In vitro fluorescence images of the GIT and five principal organs from mice receiving oral administration of P127M@DiRs (DiR, 10 μM) at different time points (12, 24, 48, and 72 h). e) Quantification of the relative MFIs of colons using Image J software. f) CLSM images of colon sections from UC mice receiving oral administration of P127M@DiOs (DiO, 10 μM) for 12 and 24 h (Scale bar = 100 μm). Macrophages were stained with DAPI for visualization of nuclei (blue). g) CLSM images of colon sections from mice receiving the treatment of P127M@DiOs for 24 h (Scale bar = 50 μm). Tissue sections were stained with DAPI and AF647-labeled F4/80 antibodies to visualize nuclei (blue) and macrophages (red), respectively. Each point represents mean ± S.E.M. (n = 3; $^{*}p < 0.05$, $^{**}p < 0.01$, $^{***}p < 0.001$, and ns = no significance).

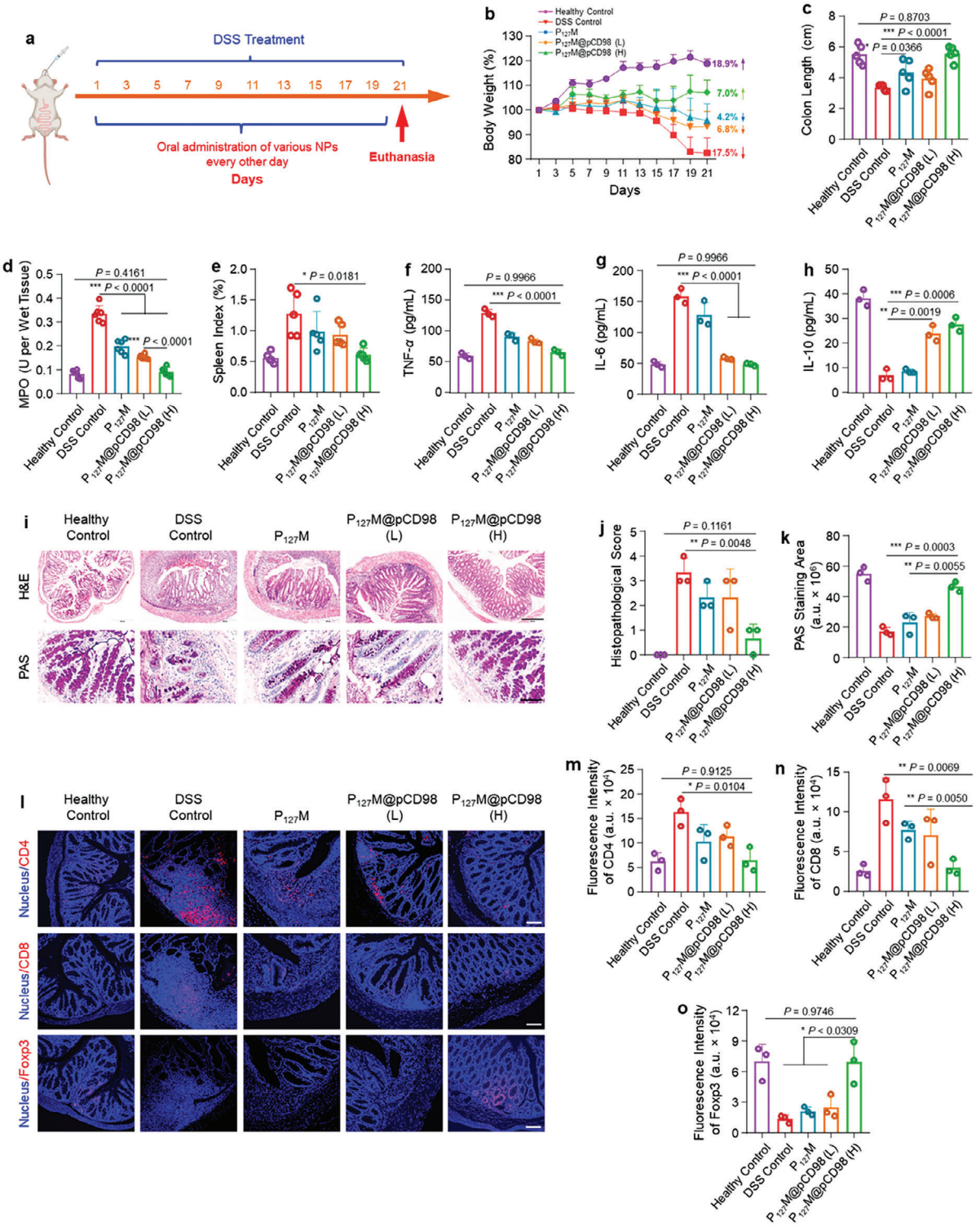

Figure 4. In vivo treatment outcomes of LNPs against DSS-induced acute UC via the oral route. a) Schematic diagram of acute UC establishment and treatment process. b) Body weight variations during the entire investigation. c) Colon lengths, d) colonic MPO activities, and e) spleen weights of various treatment groups at the end of experiments. Each point represents mean ± S.E.M. (n = 5; $^{*}p < 0.05$, $^{**}p < 0.01$, $^{***}p < 0.001$, and ns = no significance). Concentrations of f) TNF-α, g) IL-6, and h) IL-10 in the colon homogenates were quantified by their corresponding ELISA kits. (i) H&E- (Scale bar = 200 μm) and PAS-stained (Scale bar = 50 μm) colon tissue sections. Quantitative results of (j) H&E- and k) PAS-stained colon tissue sections. l) Immunofluorescence staining of CD4+ T cells, CD8+ T cells, and Foxp3+ cells in the colon tissues (scale bar = 100 μm). Quantitative analysis of (m) CD4+ T cells, n) CD8+ T cells, and o) Foxp3+ cells in the colon tissues. Each point represents mean ± S.E.M. (n = 3; $^{*}p < 0.05$, $^{**}p < 0.01$, $^{***}p < 0.001$, and ns = no significance).

hematoxylin and eosin (H&E). It was observed that the colitis signs, such as crypt disappearance, epithelial layer injury, goblet cell depletion, and immune cell infiltration, were observed in the colon tissues from the DSS control group. In contrast, all these inflammatory signs were alleviated in the $P_{127}M$, $P_{127}M$@pCD98 (L), and $P_{127}M$@pCD98 (H) groups (Figure 4i). The colon morphology of the $P_{127}M$@pCD98 (H) group was similar to that of the healthy control group, as confirmed by histological scores (Figure 4j). Mucus is a vital protective layer for the underlying colonic mucosa but has also been considered an obstacle for oral drugs. We determined that the DSS control group had the lowest amount of mucin glycoproteins in its colon tissues, which was in good agreement with the depletion patterns of goblet cells (Figure 4i,k). The LNP treatments significantly promoted mucus secretion, and the $P_{127}M$@pCD98 (H) treatment presented the most potent capacity to recover mucus secretion. Colonic tight junctions are essential for maintaining mucosal barrier integrity and the compact structure of colonic mucosa. Therefore, we determined whether oral LNPs could increase the expression profiles of the primary tight junction proteins (ZO-1 and MUC2) in the colon. DSS reduced the levels of ZO-1 and MUC2, while LNP treatments increased their expressions in the colon tissues (Figure S11, Supporting Information). Among all DSS-treated groups, the $P_{127}M$@pCD98 (H) group showed the most green (ZO-1) and red (MUC2) fluorescence, demonstrating that oral $P_{127}M$@pCD98s (H) could alleviate DSS-induced damage to the colonic epithelial barrier through increased expression of colonic tight junctions.

Extensive $CD4^+$ and $CD8^+$ T lymphocyte infiltration was reported in the colonic mucosa of UC mice and UC patients.[29] These cells are central to colon tissue damage, intestinal inflammation, and tumorigenesis.[30] However, regulatory T lymphocytes (Tregs) have been shown to possess immunomodulatory functions that suppress immune responses.[31] As shown in Figure 4l, colon tissue sections from the DSS control group showed increased red fluorescence of both $CD4^+$ and $CD8^+$ T lymphocytes; however, oral treatment with $P_{127}M$@pCD98s (H) significantly decreased their numbers in the colon tissues (Figure 4m,n). We also observed that the $P_{127}M$@pCD98 (H) group had the largest number of $Foxp3^+$ Tregs among all DSS-treated groups (Figure 4o), comparable to that of the healthy control. Additionally, blood parameters were measured (Figure S12, Supporting Information), organ indices were determined (Figure S13, Supporting Information), and sections from the five principal organs were examined (Figure S14, Supporting Information). We found no statistically significant difference between the healthy control group and the $P_{127}M$@pCD98 (H) group concerning these parameters and tissue morphologies, which demonstrates the excellent biosafety of orally administered $P_{127}M$@pCD98 (H).

The above findings confirm that oral $P_{127}M$@pCD98s (H) can retard body weight loss, colon length shortening, mucus reduction, epithelial layer damage, spleen increase, and immune system activation, which might be ascribed to their capacity to down-regulate inflammatory reactions by the anti-inflammatory lipids in MLLs and *CD98* editing, decrease infiltration of $CD4^+$ and $CD8^+$ T lymphocytes, and increase infiltration of $Foxp3^+$ Tregs.

2.7. Impacts of LNPs on Intestinal Microbiota and Gene Expression during Retardation of Acute UC

The composition of intestinal microbiota is closely associated with the development of colon diseases.[3,32] Therefore, we determined its profiles by 16S rRNA sequencing. The Venn diagram showed that 123 of the 456 operational taxonomic units (OTUs) were shared among the five groups, and there was a 167 species overlap among the 216 species between the healthy control group and the $P_{127}M$@pCD98 (H) group. Notably, the number of bacterial species at the OTU level decreased in the DSS control group, whereas LNP treatment increased the number of bacterial species (Figure S15a, Supporting Information). Alpha diversity analysis reflected the diversity of microorganisms in the intestinal ecosystem. In comparison with the healthy control group, the intestinal microbial composition of the DSS control group was changed at the Order level (**Figure 5a**; Figure S15b, Supporting Information). Interestingly, the intestinal microbial composition of the $P_{127}M$@pCD98 (H) group was similar to that of the healthy control. Principal component analysis (PCA) revealed the different microbial compositions in various groups (Figure 5b). The healthy control group and the $P_{127}M$@pCD98 (H) group showed a pronounced overlap, verifying the similarity in microbial composition between these two groups. These findings are represented by the heatmap (Figure S15c, Supporting Information). We also found that oral $P_{127}M$@pCD98s (H) greatly increased the abundance of beneficial bacteria (e.g., *Muribaculaceae*, *Prevotellaceae*, and *Bacteroidaceae*) and decreased the harmful bacteria (e.g., *Pasteurellaceae*, *Aerococcaceae*, and *Helicobacteraceae*) (Figure 5c,d).

The molecular mechanism of $P_{127}M$@pCD98's effectiveness in alleviating UC was determined at the gene expression level. A total of 16248 expressed genes were identified, including 13506 commonly expressed genes, 392 typical genes in the healthy control group, 428 typical genes in the DSS control group, 177 typical genes in the $P_{127}M$ group, and 228 typical genes in the $P_{127}M$@pCD98 (H) group (Figure 5e). The volcano plots revealed 586 up-regulated and 1284 down-regulated differentially expressed genes (DEGs) (healthy control vs DSS control), 53 up-regulated and 378 down-regulated DEGs ($P_{127}M$ vs DSS control), and 291 up-regulated and 1025 down-regulated DEGs ($P_{127}M$@pCD98 (H) vs DSS control), suggesting that the gene expression profile of the $P_{127}M$ group was more similar to that of the DSS control group than the $P_{127}M$@pCD98 (H) group (Figure S16a-c, Supporting Information). These DEGs were involved in various cellular processes, such as immune responses, metabolic processes, and cell junctions (Figure S16d, Supporting Information). KEGG enrichment analysis confirmed that the significant DEGs after $P_{127}M$@pCD98 treatment were enriched in the signaling pathways associated with infection, immune response, cell proliferation, cell migration, *C*-type lectin receptor, growth hormone secretion, and vascular endothelial growth factor (Figure 5g).

We found that the expression of CD98 heavy chain (CD98hc, encoded by *SLC3A2*) was down-regulated in the $P_{127}M$@pCD98 group compared with the DSS control group (Figure S17, Supporting Information). CD98hc is a type II transmembrane protein covalently linked to one of *L*-type amino acid transporters (light chain).[33] CD98hc, a regulatory factor for integrins, causes

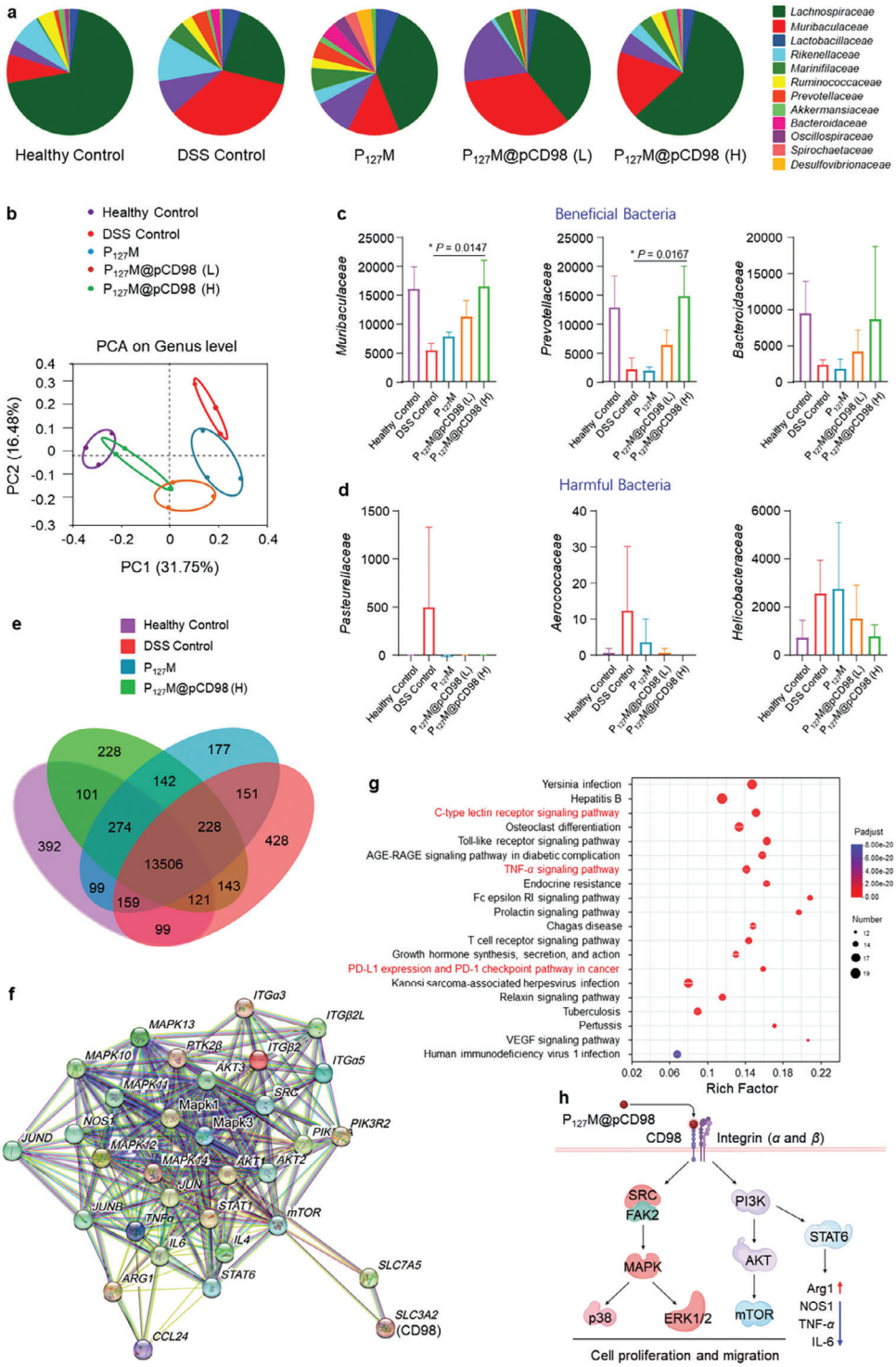

Figure 5. The impact of oral LNPs on intestinal microbial populations and colon tissue gene expression profiles. a) Compositions of intestinal microbiota at the Order level. b) PCA of intestinal microbiota from various treatment groups. Variations of the typical c) beneficial and d) harmful bacteria in the intestinal microbiota from various treatment groups. e) Venn diagram of the numbers of differentially expressed genes in various treatment groups. f) Interaction network of differentially expressed genes relevant to anti-inflammation and epithelial repair after CD98 knockout by oral LNPs. g) Enriched KEGG pathways of differentially expressed genes relevant to anti-inflammation and epithelial repair after CD98 knockout by oral LNPs. Each point represents mean ± S.E.M. (n = 3; $^{*}p < 0.05$, $^{**}p < 0.01$, $^{***}p < 0.001$, and ns = no significance). h) Scheme illustration of the therapeutic mechanism of P127M@pCD98s against UC.

integrin β1 to aggregate into high-density complexes, activating integrin and promoting integrin-like signal transduction, nonadherent growth, and intestinal inflammation. The *CD98* knockdown by oral P_{127}M@pCD98s facilitated the expression of sparse representation-based classifier (SRC) and focal adhesion kinase 2 (FAK2), induced the activated integrin-like signaling pathway, and boosted colonic epithelial reconstruction by the activation of downstream ERK1/2 and p38MAPK signal pathways, leading to colitis alleviation (Figure 5f–h). The *CD98* knockdown also increased the production of galectin-3, which activated the phosphatidylinositol 3-kinase PI3K/signal transducers and transcription (STAT6) signaling pathway, promoting macrophage polarization to the anti-inflammatory M2 phenotype.

2.8. In Vivo Therapeutic Effect of LNPs on Chronic UC

IL-10 can inhibit inflammatory reactions and promote immune homeostasis. IL-10 knockout mice spontaneously develop UC, and they have been used as a model of chronic colitis. We used this mouse model to determine whether oral P_{127}M@pCD98s could exert therapeutic effects against chronic colitis (**Figure** 6a). Figure 6b showed a slight body weight loss (2.8%) in the control mice, whereas the treatment groups gained weight; the P_{127}M@pCD98 (H) group had the largest body weight gain (3.9%). The colon morphology (Figure S18, Supporting Information) and colon length (Figure 6c) suggested that the LNP treatments significantly retarded colon shortening compared with the control group, and the P_{127}M@pCD98 (H) group exhibited markedly longer colon lengths than the other groups. We also found that oral treatment with P_{127}M@pCD98s (H) yielded the lowest MPO level, spleen index, and pro-inflammatory cytokine (TNF-α and IL-6) concentrations (Figure 6d–g).

The pathological changes in the colon tissues from different mouse groups were evaluated after H&E staining (Figure 6h), and the control group presented obvious colitis symptoms, such as damage to the colonic epithelial barriers, infiltration of immune cells, and depletion of goblet cells. However, oral administration of NPs alleviated these symptoms. The colon tissues from the P_{127}M@pCD98 (H) group exhibited complete histological microstructures with no infiltration of inflammatory cells, and the histological score was lower than those of the other groups (Figure 6i). Compared with the control group, the treatment groups had increased mucus amounts, with the P_{127}M@pCD98 (H) group showing the most significant mucin quantity (Figure 6j). It was observed that the green fluorescence signal of ZO-1 in the colon tissues from the P_{127}M@pCD98 (H) group was more extensive than those from the other groups (Figure 6k,l), and oral P_{127}M@pCD98s (H) significantly increased the secretion of MUC2 (Figure 6m). Thus, treatment with the various NPs, especially P_{127}M@pCD98s (H), effectively increased mucin production, restored the mucus layer, and promoted the integrity of the colonic epithelial barrier.

$CD4^+$ and $CD8^+$ T lymphocytes are activated in colitis patients, whose transcriptional profiles can be used to predict the active state of colitis.[34] Figure 6n-q indicated that the control group showed strong red fluorescence intensities of $CD4^+$ and $CD8^+$ T cells, and the trend of $Foxp3^+$ Tregs was opposite to those of $CD4^+$ and $CD8^+$ T cells. The P_{127}M@pCD98 (H) group presented the lowest proportion of $CD4^+$ and $CD8^+$ T cells and the highest proportion of $Foxp3^+$ Tregs. These results demonstrate that oral P_{127}M@pCD98s (H) significantly inhibit inflammatory responses by down-regulating $CD4^+$ and $CD8^+$ T cells and up-regulating $Foxp3^+$ Tregs in the colon tissues. We also found that P_{127}M@pCD98 (H) treatment decreased the numbers of several immune cell types, including the white blood cell count (WBC), lymphocytes, granulocytes, and monocytes (Figure S19, Supporting Information), indicating that P_{127}M@pCD98s (H) could efficiently down-regulate the activation of immune cells involved in the exacerbation of colitis. In addition, the low organ indices (Figure S20, Supporting Information) and normal tissue morphologies of the five principal organs (Figure S21, Supporting Information) confirmed the negligible toxicity of oral P_{127}M@pCD98s (H).

2.9. In Vivo Therapeutic Effect of LNPs on CAC

The murine model of CAC induced by azoxymethane (AOM)/DSS was used to evaluate whether oral LNPs could prevent the development of CAC (**Figure** 7a). After 42 days of induction, the AOM/DSS control group showed a body weight loss of 2.4%, which was reversed by oral administration of P_{127}Ms and P_{127}M@pCD98s (Figure 7b). Relative to the AOM/DSS control, oral P_{127}M@pCD98s significantly increased colon length (Figure 7c) and decreased total tumor numbers (Figure 7d), tumor distribution ranges (Figure 7e; Figure S22, Supporting Information), MPO values (Figure 7f), and spleen indices (Figure 7g). Oral P_{127}M@pCD98s decreased the levels of pro-inflammatory cytokines (TNF-α and IL-6), while increasing the expression of an anti-inflammatory factor, IL-10 (Figure 7h–j).

H&E staining and examination revealed that the AOM/DSS control group showed the highest level of colonic carcinoma, which was decreased by oral P_{127}M@pCD98s (Figure S23, Supporting Information). The colon tissues from the AOM/DSS control had significantly lower amounts of MUC2 compared with the other treatment groups, and the P_{127}M@pCD98 group displayed the highest amounts of colonic mucus among all treatment groups. The above results demonstrate that P_{127}M@pCD98s have the strongest capacity to restore mucin secretion. ZO-1 showed the same production trend as MUC2, suggesting that P_{127}M@pCD98s could alleviate the damage to the colonic epithelial barrier by increasing ZO-1 expression (Figure S24, Supporting Information). As seen in Figure S25 (Supporting Information), large numbers of $CD4^+$ T cells infiltrated the colorectal tumor tissues in the P_{127}M@pCD98 group, which would be beneficial by retarding the tumor growth. $CD8^+$ T cells can induce colon tissue damage and intestinal inflammation, which could initiate and accelerate tumorigenesis. We found that P_{127}M@pCD98 treatment significantly decreased the number of colonic $CD8^+$ T cells to a level comparable to that of the healthy control group. $Foxp3^+$ Tregs can restore the damaged colonic epithelial barrier and promote colonic homeostasis, and treatment with P_{127}Ms and P_{127}M@pCD98s could enhance the accumulation of $Foxp3^+$ Tregs in the colon tissues. Additionally, the P_{127}M@pCD98 group showed blood parameters (Figure S26, Supporting Information) and organ indices (Figure S27, Supporting Information)

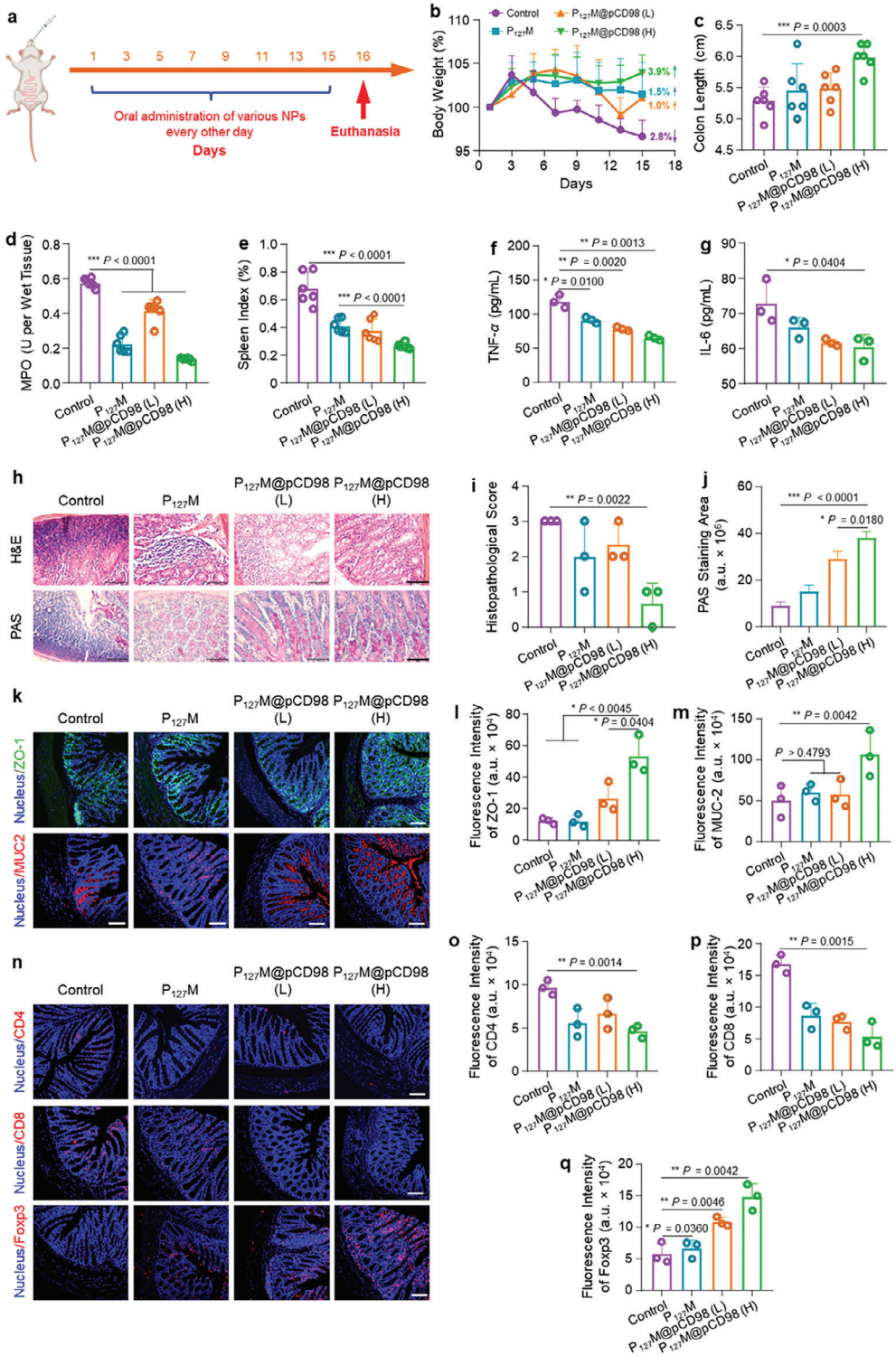

Figure 6. In vivo treatment outcomes of LNPs against chronic UC in IL-10 knockout mice via the oral route. a) Schematic diagram of the treatment process. b) Body weight variations during the entire investigation. c) Colon lengths, d) colonic MPO activities, and e) spleen weights of various treatment groups at the end of experiments. Each point represents mean ± S.E.M. (n = 5; $^{*}p < 0.05$, $^{**}p < 0.01$, $^{***}p < 0.001$, and ns = no significance). Their corresponding ELISA kits quantified concentrations of f) TNF-α and g) IL-6 in the colon homogenates. h) H&E- and PAS-stained colon tissue sections (Scale bar = 50 μm). Quantitative results of i) H&E- and j) PAS-stained colon tissue sections. k) Immunofluorescent staining of ZO-1 and MUC2 in the colon tissues (scale bar = 100 μm). Quantitative analysis of l) ZO-1 and m) MUC2 in the colon tissues. n) Immunofluorescence staining of CD4+ T cells, CD8+ T cells, and Foxp3+ cells in the colon tissues (scale bar = 100 μm). Quantitative analysis of (o) CD4+ T cells, (p) CD8+ T cells, and (q) Foxp3+ cells in the colon tissues. Each point represents mean ± S.E.M. (n = 3; $^{*}p < 0.05$, $^{**}p < 0.01$, $^{***}p < 0.001$, and ns = no significance).

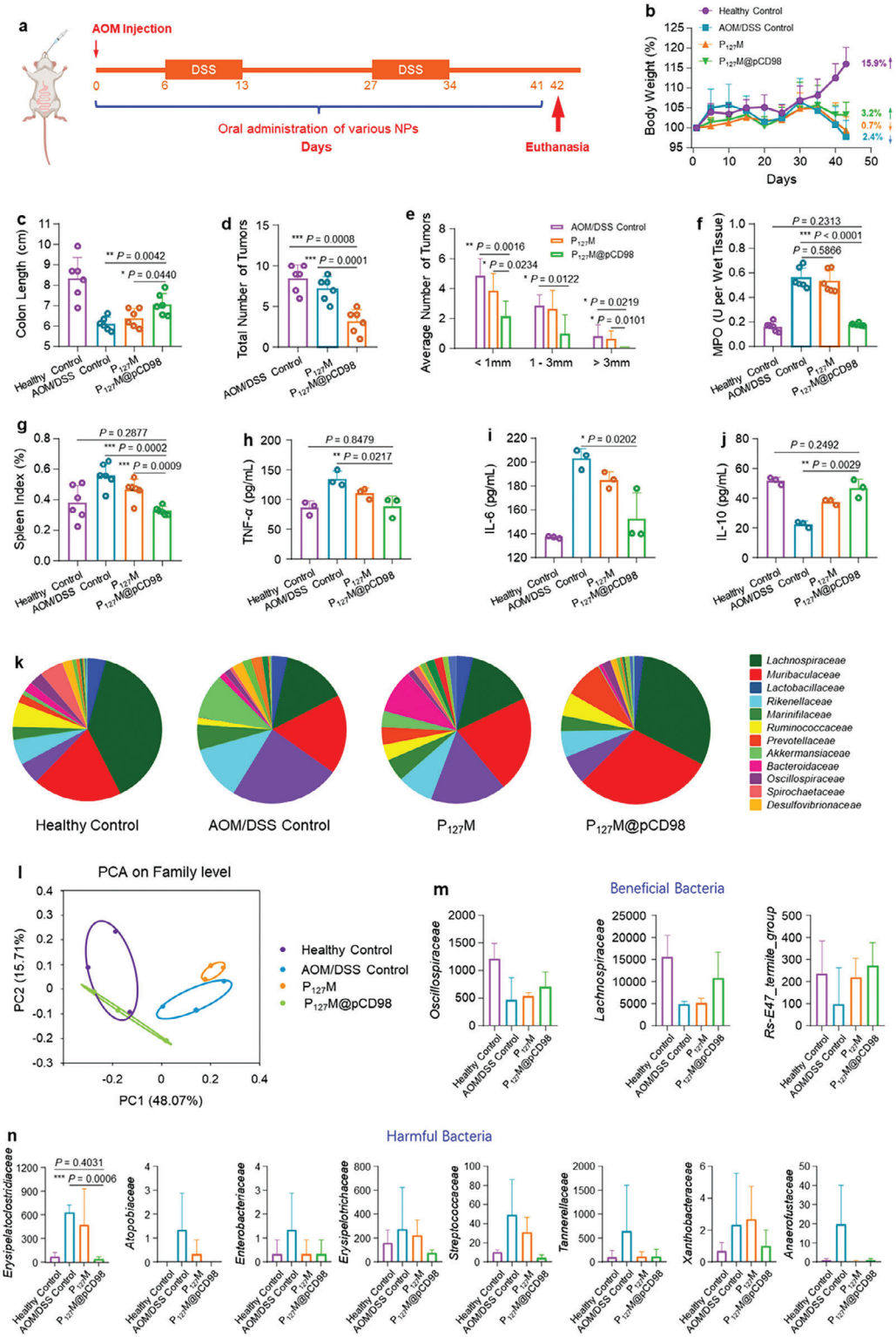

Figure 7. In vivo treatment outcomes of LNPs against AOM/DSS-induced CAC via the oral route. a) Schematic diagram of CAC establishment and treatment process. b) Body weight variations during the entire investigation. c) Colon lengths, d) total tumor numbers, e) tumor size distributions, f) colonic MPO activities, and g) spleen indexes of various treatment groups at the end of experiments. Each point represents mean ± S.E.M. (n = 6; $^{*}p < 0.05$, $^{**}p < 0.01$, $^{***}p < 0.001$, and ns = no significance). Concentrations of h) TNF-α, (i) IL-6, and (j) IL-10 in the colon homogenates were quantified by their corresponding ELISA kits. k) Intestinal microbiota compositions from various treatment groups at the Order level. l) PCA of intestinal microbiota from various treatment groups. Variations of the typical (m) beneficial and n) harmful bacteria in the intestinal microbiota from various treatment groups. Each point represents mean ± S.E.M. (n = 3; $^{*}p < 0.05$, $^{**}p < 0.01$, $^{***}p < 0.001$, and ns = no significance).

comparable to those in the healthy control group, and this treatment group caused negligible toxicities to the five principal organs (Figure S28, Supporting Information).

DSS treatment reduced the microbial richness (Chao index) and ecological dominance (Sbos index) (Figure S29a,b, Supporting Information); however, oral LNPs significantly increased bacterial richness and diversity. It was found that 232 of the 456 OTUs were shared among the four groups, and there was an overlap of 313 OTUs among the 436 OTUs between the healthy control group and the P_{127}M@pCD98 group. Notably, 31 OTUs were unique in the P_{127}M@pCD98 group, and the number of microbial species in this group was increased at the OTU level (Figure S29c, Supporting Information). The intestinal microbial composition of the AOM/DSS control group differed at the Order level (Figure 7k; Figure S27d, Supporting Information) compared with the healthy control group. The P_{127}M@pCD98 group had microbial compositions similar to the healthy control group, as verified by PCA (Figure 7l) and heatmap (Figure S29e, Supporting Information) results. Figure 7m,n showed that oral P_{127}M@pCD98s increased the proportions of typical beneficial bacteria such as *Oscillospiraceae*, *Lachnospiraceae*, and the *Rs-E47_termite*_group, and decreased the numbers of harmful bacteria, *Erysipelatoclostridiaceae*, *Atopobiaceae*, and *Enterobacteriaceae*. These results confirm that oral administration of P_{127}M@pCD98s can sustain intestinal microbial homeostasis, which is beneficial for the retardation of CAC.

3. Conclusion

In this study, we developed an oral CRISPR/Cas9 delivery platform based on edible mulberry leaf lipids and Pluronic F127. The resultant lipid nanoparticles (P_{127}M@pCD98s) maintained stability during passage through the gastrointestinal tract, infiltrated through the mucus barrier, and penetrated the colitis tissues and colorectal tumor tissues. P_{127}M@pCD98s could be specifically internalized by macrophages via galactose receptor-mediated endocytosis and subsequently escape from lysosomes. In vitro experiments suggested that P_{127}M@pCD98s mitigated inflammatory responses through down-regulation of CD98 expression, polarization of macrophages to the anti-inflammatory M2 phenotype, and decreased release of TNF-α and IL-6. Oral administration of P_{127}M@pCD98s efficiently retarded the progression of ulcerative colitis and colitis-associated colorectal cancer, enriched the beneficial bacteria, and reduced the abundance of harmful bacteria. Collectively, these results demonstrate, for the first time, the feasibility of LNPs (P_{127}Ms) as an oral CRISPR/Cas9 delivery platform, which could be exploited for effective oral treatment of colon diseases.

4. Experimental Section

Preparation of Various NPs: MLLs were extracted from fresh mulberry leaves, according to the previous report. Their lipid compositions and molecular species were analyzed by liquid chromatography coupled to tandem mass spectrometry (LC–MS/MS, Thermo Electron, San Jose, CA, USA) and reversed-phase high-performance liquid chromatography (UPLC, BEH C18 chromatography column, 100 × 2.1 mm, 1.7 µm, Waters Corp., Milford, MA, USA), respectively. The organic phase containing MLLs was mixed with various Pluronic polymer solutions (MLL/Pluronic polymer = 100:5, w/w), and the mixtures were dried into a film at 37 °C using a rotary evaporator (Shanghai Sensichip Infotech Co. Ltd, Shanghai, China). Thereafter, plasmid aqueous solution was added to the round-bottom flask containing MLL/Pluronic film and sonicated in a water bath at 100 W for 2 min. Finally, the obtained NPs were resuscitated by adding HEPES buffer (20 µmol L^{-1}, 2 mL) and stored at −20°C for further applications.

In Vitro Transfection Efficiency of Various NPs: Raw 264.7 macrophages and CT-26 cells were inoculated into 12-well plates with a cell density of 1.0×10^5 cells per well and cultured overnight. The complete medium was replaced with a basic medium containing different LNPs (equivalent to 1 µg pGFP). After incubation for 6 h, a complete medium (1 mL) was added to each well and further co-incubated for 24 and 48 h, respectively. Subsequently, the medium was discarded, and cells were washed with PBS 3 times. The green fluorescence signals of GFP in the cells were detected by CLSM (FV3000, Olympus, Japan), and the transfection efficiencies of various NPs were quantified by FCM (Beckman Coulter Inc, USA).

In Vitro Anti-Inflammatory Activities of LNPs: Raw 264.7 macrophages were inoculated into 12-well plates with a cell density of 1.0×10^5 cells per well and cultured overnight. The complete medium was replaced with an essential medium containing different LNPs (equivalent to 1 µg pCD98). After incubation for 6 h, a complete medium (1 mL) was added to each well and further co-incubated for 48 h. The cells were washed with PBS 3 times and treated with LPS (0.5 µg mL^{-1}) for 3 h. The supernatants in the wells were collected and centrifuged at 3,000 *g* for 10 min. Finally, the concentrations of pro-inflammatory and anti-inflammatory cytokines were quantified by the corresponding enzyme-linked immunosorbent assay (ELISA) kits (Solarbio Life Science, Beijing, China).

Experimental Animals: All animals were free to obtain water and food, and the state of animal hair and feces were observed every day. All the experimental protocols were in accordance with the Institutional Animal Care and Use Committee of Southwest University (IACUC-20210310-09).

In Vivo Therapeutic Effect of NPs against Chronic Colitis: IL-10 knockout C57/BL6 mice (20-22 weeks old, female, Shanghai Model Organisms Center, Inc., Shanghai, China) were randomly divided into 4 groups: the control group, P_{127}M group, P_{127}M@pCD98 (L, 1 µg pCD98 per mouse) group, and P_{127}M@pCD98 (H, 5 µg pCD98 per mouse) group. The P_{127}M amount used in the P_{127}M group was equal to that in the P_{127}M@pCD98 (H) group. Mouse body weights were recorded every day throughout the experiment. At the end of the treatment, colons, major organs, and feces were collected and weighed. Blood routine test and colonic MPO activity were measured by a hematology analyzer (BC-2800VET, Mindray, Guangdong, China) and MPO kit. The concentrations of pro-inflammatory cytokines (TNF-α and IL-6) and anti-inflammatory cytokines (IL-10) in the colon tissues were measured with their corresponding ELISA kits (Solarbio Life Science, Beijing, China).

To observe the therapeutic outcomes of each treatment at the tissue level, the collected colon tissues were fixed in formalin solution, embedded in paraffin, cut into sections (5 µm), and stained with H&E and PAS kits. $CD4^+$ T cells, $CD8^+$ T cells, $Foxp3^+$ regulatory T cells, and tight junction proteins (ZO-1 and MUC2) were stained with their corresponding fluorescent antibodies (Wuhan Servicebio Technology Co., Ltd, Wuhan, China). Tissue sections were imaged using a CLSM (FV3000, Olympus, Japan).

In Vivo Therapeutic Effect of NPs against CAC: BalB/c mice (6-8-week-old male) were from Ernsville Experimental Animals Co., Ltd., Chongqing, China. The CAC mouse model was established according to the previous studies.[27,35] Briefly, mice were intraperitoneally injected with AOM (10 mg Kg^{-1}) and maintained for 7 days. Subsequently, mice received 2 cycles of drinking water containing DSS (3.5%, w/v). Mice were divided into four groups: the healthy control group, the AOM/DSS control group, the P_{127}M group, and the P_{127}M@pCD98 (5 µg pCD98 per mouse) group. The P_{127}M amount used in the P_{127}M group was equal to that in the P_{127}M@pCD98 (5 µg pCD98 per mouse) group. Mouse body weights were recorded every day throughout the experiment. At the end of the treatment, colons, major organs, and feces were collected and weighed, and the numbers and size distributions of tumors in each group were statistically analyzed. Blood routine test and colonic MPO activity were measured by hematology analyzer (BC-2800VET, Mindray, Guangdong, China)

and MPO kit. The concentrations of pro-inflammatory cytokines (TNF-α and IL-6) and anti-inflammatory cytokines (IL-10) in the colon tissues were quantified with their corresponding ELISA kits (Solarbio Life Science, Beijing, China).

Statistical Analysis: Statistical analysis was conducted using a student's *t*-test or ANOVA test, followed by a Bonferroni post-hoc test (GraphPad Prism). Data were presented as mean ± standard error of the mean (S.E.M.). Statistical significance was expressed by $^{*}p < 0.05$, $^{**}p < 0.01$, and $^{***}p < 0.001$.

Supporting Information

Supporting Information is available from the Wiley Online Library or from the author.

Acknowledgements

This study was supported by the National Natural Science Foundation of China (82072060, 82360110, and 22008201), the Science and Technology Department of Jiangxi Province (20212BDH81019 and 20224BAB206073), the Fundamental Research Funds for the Central Universities (SWU-XDPY22006 and SWU-KQ22075), the Venture & Innovation Support Program for Chongqing Overseas Returnees (2205012980212766), and the Science Fund for Distinguished Young Scholars of Chongqing Municipality (2022NSCQ-JQX5279).

Conflict of Interest

The authors declare no conflict of interest.

Data Availability Statement

The data that support the findings of this study are available from the corresponding author upon reasonable request.

Keywords

colon disease, CRISPR/Cas9, macrophage-targeting, oral administration, plant lipid nanoparticles

Received: August 22, 2023
Revised: December 14, 2023
Published online:

[1] B. Xiao, H. Laroui, E. Viennois, S. Ayyadurai, M. A. Charania, Y. Zhang, Z. Zhang, M. T. Baker, B. Zhang, A. T. Gewirtz, D. Merlin, *Gastroenterology* **2014**, *146*, 1289.
[2] P. Jaaks, E. A. Coker, D. J. Vis, O. Edwards, E. F. Carpenter, S. M. Leto, L. Dwane, F. Sassi, H. Lightfoot, S. Barthorpe, D. Van Der Meer, W. Yang, A. Beck, T. Mironenko, C. Hall, J. Hall, I. Mali, L. Richardson, C. Tolley, J. Morris, F. Thomas, E. Lleshi, N. Aben, C. H. Benes, A. Bertotti, L. Trusolino, L. Wessels, M. J. Garnett, *Nature* **2022**, *603*, 166.
[3] K. Zhang, L. Zhu, Y. Zhong, L. Xu, C. Lang, J. Chen, F. Yan, J. Li, J. Qiu, Y. Chen, D. Sun, G. Wang, K. Qu, X. Qin, W. Wu, *Adv. Sci.* **2023**, *10*, e2205422.
[4] P. J. Coombs, M. E. Taylor, K. Drickamer, *Glycobiology* **2006**, *16*, 1C.
[5] V. Ranganathan, K. Wahlin, J. Maruotti, D. J. Zack, *Nat. Commun.* **2014**, *5*, 4516.
[6] Z. Chang, Y. Wang, C. Liu, W. Smith, L. Kong, *Stem Cell Res Ther* **2020**, *15*, 559.
[7] K. Paunovska, D. Loughrey, J. E. Dahlman, *Nat. Rev. Genet.* **2022**, *23*, 265.
[8] B. B. Mendes, J. Conniot, A. Avital, D. Yao, X. Jiang, X. Zhou, N. Sharf-Pauker, Y. Xiao, O. Adir, H. Liang, J. Shi, A. Schroeder, J. Conde, *Nat. Rev. Dis. Primers* **2022**, *2*, 24.
[9] D. Ambort, M. E. V. Johansson, J. K. Gustafsson, H. E. Nilsson, A. Ermund, B. R. Johansson, P. J. B. Koeck, H. Hebert, G. C. Hansson, *Proc. Natl. Acad. Sci. U.* **2012**, *109*, 5645.
[10] L. M. Ensign, C. Schneider, J. S. Suk, R. Cone, J. Hanes, *Adv. Mater.* **2012**, *24*, 3887.
[11] L. M. Ensign, R. Cone, J. Hanes, *Adv. Drug Delivery Rev.* **2012**, *64*, 557.
[12] C. Zhao, J. Yang, M. Chen, W. Chen, X. Yang, H. Ye, L. Wang, Y. Wang, J. Shi, F. Yue, X. Ma, *ACS Nano* **2023**, *17*, 811.
[13] P. Zhao, X. Xia, X. Xu, K. K. C. Leung, A. Rai, Y. Deng, B. Yang, H. Lai, X. Peng, P. Shi, H. Zhang, P. W. Y. Chiu, L. Bian, *Nat. Commun.* **2021**, *12*, 7162.
[14] a) Q. Chen, Q. Li, Y. Liang, M. Zu, N. Chen, B. S. B. Canup, L. Luo, C. Wang, L. Zeng, B. Xiao, *Acta Pharmacol Sin* **2022**, *12*, 907; b) Q. Chen, M. Zu, H. Gong, Y. Ma, J. Sun, S. Ran, X. Shi, J. Zhang, B. Xiao, *J. Nanobiotechnol.* **2023**, *21*, 6; c) M. Zhang, E. Viennois, M. Prasad, Y. Zhang, L. Wang, Z. Zhang, M. K. Han, B. Xiao, C. Xu, S. Srinivasan, D. Merlin, *Biomaterials* **2016**, *101*, 321.
[15] Y. Lee, N. Kamada, J. J. Moon, *Adv. Drug Delivery Rev.* **2021**, *179*, 114021.
[16] B. A. H. Smith, C. R. Bertozzi, *Nat. Rev. Drug Discovery* **2021**, *20*, 217.
[17] K. V. Mariño, A. J. Cagnoni, D. O. Croci, G. A. Rabinovich, *Nat. Rev. Drug Discovery* **2023**, *22*, 295.
[18] M. Klichinsky, M. Ruella, O. Shestova, X. M. Lu, A. Best, M. Zeeman, M. Schmierer, K. Gabrusiewicz, N. R. Anderson, N. E. Petty, K. D. Cummins, F. Shen, X. Shan, K. Veliz, K. Blouch, Y. Yashiro-Ohtani, S. S. Kenderian, M. Y. Kim, R. S. O'connor, S. R. Wallace, M. S. Kozlowski, D. M. Marchione, M. Shestov, B. A. Garcia, C. H. June, S. Gill, *Nat. Biotechnol.* **2020**, *38*, 947.
[19] E. I. Buzas, *Nat. Rev. Microbiol.* **2023**, *23*, 236.
[20] Y. Kong, F. Liu, B. Ma, J. Duan, W. Yuan, Y. Sang, L. Han, S. Wang, H. Liu, *Adv. Sci.* **2021**, *8*, 2100962.
[21] J. Lan, L. Sun, F. Xu, L. Liu, F. Hu, D. Song, Z. Hou, W. Wu, X. Luo, J. Wang, X. Yuan, J. Hu, G. Wang, *Cancer Res.* **2019**, *79*, 146.
[22] a) Q. Zhou, D. F. Niño, Y. Yamaguchi, S. Wang, W. B. Fulton, H. Jia, P. Lu, T. Prindle Jr., D. Pamies, M. Morris, L. L. Chen, C. P. Sodhi, D. J. Hackam, *Sci. Transl. Med.* **2021**, *13*, 6412; b) N. Yaghoubi, A. Soltani, K. Ghazvini, S. M. Hassanian, S. I. Hashemy, *Biomed. Pharmacother.* **2019**, *110*, 312.
[23] Y. Wu, Y. Li, Z. Ruan, J. Li, L. Zhang, H. Lu, Z. Xu, *J. Agric. Food Chem.* **2020**, *68*, 11402.
[24] G. M. H. Birchenough, B. O. Schroeder, S. Sharba, L. Arike, C. V. Recktenwald, F. Puértolas-Balint, M. V. Subramani, K. T. Hansson, B. Yilmaz, S. K. Lindén, F. Bäckhed, G. C. Hansson, *Cell Rep.* **2023**, *42*, 112084.
[25] P. Paone, P. D. Cani, *Gut* **2020**, *69*, 2232.
[26] T. Breugelmans, B. Oosterlinck, W. Arras, H. Ceuleers, J. De Man, G. L. Hold, B. Y. De Winter, A. Smet, *Lancet Gastroenterol* **2022**, *7*, 455.
[27] M. Zu, D. Xie, B. S. B. Canup, N. Chen, Y. Wang, R. Sun, Z. Zhang, Y. Fu, F. Dai, B. Xiao, *Biomaterials* **2021**, *279*, 121178.
[28] C. F. Krieglstein, W. H. Cerwinka, F. S. Laroux, M. B. Grisham, G. Schürmann, M. Brüwer, D. N. Granger, *J. Surg. Res.* **2001**, *101*, 166.
[29] D. Fujiwara, L. Chen, B. Wei, J. Braun, *Am J Physiol* **2011**, *300*, G939.

[30] S. Nancey, S. Holvöet, I. Graber, G. Joubert, D. Philippe, S. Martin, J.-F. Nicolas, P. Desreumaux, B. Flourié, D. Kaiserlian, *Gastroenterology* **2006**, *131*, 485.
[31] C. Cosovanu, C. Neumann, *Front Immunol* **2020**, *11*, 600973.
[32] a) R. Sender, S. Fuchs, R. Milo, *Cell* **2016**, *164*, 337; b) S. Yachida, S. Mizutani, H. Shiroma, S. Shiba, T. Nakajima, T. Sakamoto, H. Watanabe, K. Masuda, Y. Nishimoto, M. Kubo, F. Hosoda, H. Rokutan, M. Matsumoto, H. Takamaru, M. Yamada, T. Matsuda, M. Iwasaki, T. Yamaji, T. Yachida, T. Soga, K. Kurokawa, A. Toyoda, Y. Ogura, T. Hayashi, M. Hatakeyama, H. Nakagama, Y. Saito, S. Fukuda, T. Shibata, T. Yamada, *Nat. Med.* **2019**, *25*, 968.
[33] H. T. T. Nguyen, G. Dalmasso, L. Torkvist, J. Halfvarson, Y. Yan, H. Laroui, D. Shmerling, T. Tallone, M. D'amato, S. V. Sitaraman, D. Merlin, *J. Clin. Invest.* **2011**, *121*, 1733.
[34] C. Stienne, R. Virgen-Slane, L. Elmén, M. Veny, S. Huang, J. Nguyen, E. Chappell, M. O. Balmert, J.-W. Shui, M. A. Hurchla, M. Kronenberg, S. N. Peterson, K. M. Murphy, C. F. Ware, J. R. Sedý, *Cell Rep.* **2022**, *38*, 110553.
[35] a) B. Xiao, E. Viennois, Q. Chen, L. Wang, M. K. Han, Y. Zhang, Z. Zhang, Y. Kang, Y. Wan, D. Merlin, *ACS Nano* **2018**, *12*, 5253; b) Y. Cao, S. Liu, Y. Ma, L. Ma, M. Zu, J. Sun, F. Dai, L. Duan, B. Xiao, *Small* **2022**, *18*, e2203466.